JACS
JOURNAL OF THE AMERICAN CHEMICAL SOCIETY

Communication

pubs.acs.org/JACS

Interferometry and Fluorescence Detection for Simultaneous Analysis of Labeled and Unlabeled Nanoparticles in Solution

Stefan Wennmalm* and Jerker Widengren

Royal Institute of Technology, Albanova University Center, Department of Applied Physics, Experimental Biomolecular Physics, 106 91 Stockholm, Sweden

Supporting Information

ABSTRACT: A novel fluctuation spectroscopy technique based on interferometry is described. The technique, termed scattering interference correlation spectroscopy (SICS), autocorrelates the signals from the forward-scattered and transmitted laser light from nanoparticles (NPs) in solution. SICS has two important features: First, for unlabeled NPs with known refractive index, it analyzes not only the diffusion coefficient but also the effective cross section and concentration in a single measurement. Second, it can be combined with fluorescence correlation spectroscopy (FCS) for simultaneous analysis of labeled and unlabeled NPs. SICS is here demonstrated on unlabeled M13 phages and on unlabeled NPs with diameters of 210 nm down to 26 nm. It is also shown how the combination of SICS and FCS can be used to determine the fraction of fluorescent NPs in a mixture and estimate K_d from a single binding measurement.

The two most popular techniques for label-free analysis of particles in solution are dynamic light scattering[1] (DLS) and laser diffraction spectroscopy (LDS).[2] While DLS derives particle size from the diffusion coefficient, LDS measures the particles' projected cross section. However, neither of these techniques estimates the concentration of particles, and they cannot easily be combined with fluorescence techniques. In the past few years, interferometric techniques for analysis of single metal and polymer nanoparticles (NPs) and viruses have gained much interest. They offer high-sensitivity detection of unlabeled nanosized objects[3,4] but also allow metal NPs to be used as an alternative label that is free from fluorescence bleaching, blinking, and saturation.[5−8] Photothermal correlation spectroscopy[9] (PCS) and photothermal absorption correlation spectroscopy[10] (PhACS) were recently demonstrated as interferometric techniques for solution analysis of gold NPs as an alternative specific label.

Here scattering interference correlation spectroscopy (SICS) is introduced as a label-free technique in which fluctuations are likely caused by interference between the phase-shifted forward scattering from NPs and the transmitted laser light (reference beam), as in PCS and PhACS (Figure 1A). Autocorrelation of the forward-scattered and transmitted light yields information about not only the NPs' hydrodynamic radius but also their effective cross section and concentration. Furthermore, we demonstrate how the technique easily can be combined with fluorescence correlation spectroscopy (FCS) to allow simultaneous analysis of labeled and unlabeled NPs.

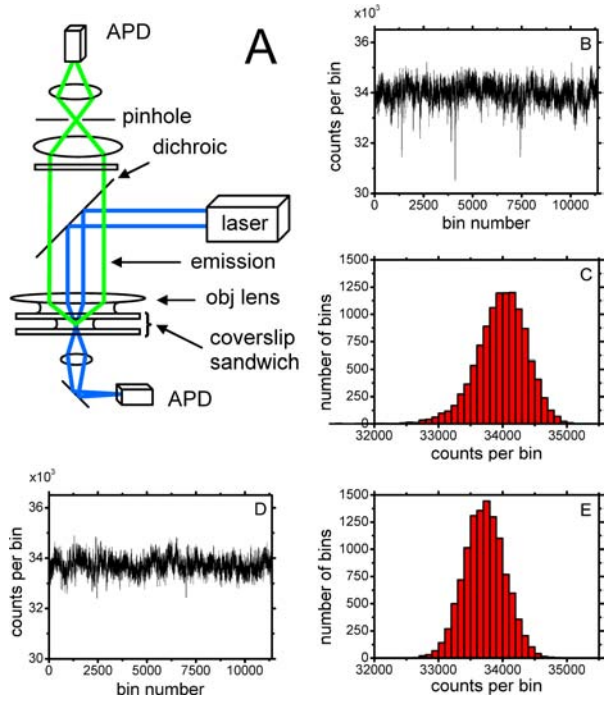

Figure 1. (A) Experimental setup for SICS and its combination with FCS. (B) Intensity trace and (C) histogram of a measurement on 93 nm NPs (bin time = 8 ms, diffusion time τ_D = 8−9 ms, N = 0.18). (D) Intensity trace and (E) histogram of a measurement on pure buffer solution (bin time = 8 ms). Measurement times were 120 s.

The autocorrelation function (ACF) amplitude is given by

$$G(0) - 1 = \frac{\langle \delta I^2(0) \rangle}{\langle I \rangle^2} \quad (1)$$

where I is the detected intensity, $\delta I(t)$ is the deviation from the mean intensity at time t, and brackets denote the mean value.

The signal caused by a single unlabeled NP is $\sigma_p P_{tot}/A_{dv} = P_{tot}A_q$, where σ_p is an effective cross section, P_{tot} is the applied laser power, A_{dv} is the area of the laser focus, and A_q is the normalized effective cross section ($A_q = \sigma_p/A_{dv}$). With a mean number of particles N in the detection volume, the fluctuation

Received: August 18, 2012
Published: November 16, 2012

   dx.doi.org/10.1021/ja308213q | J. Am. Chem. Soc. 2012, 134, 19516−19519

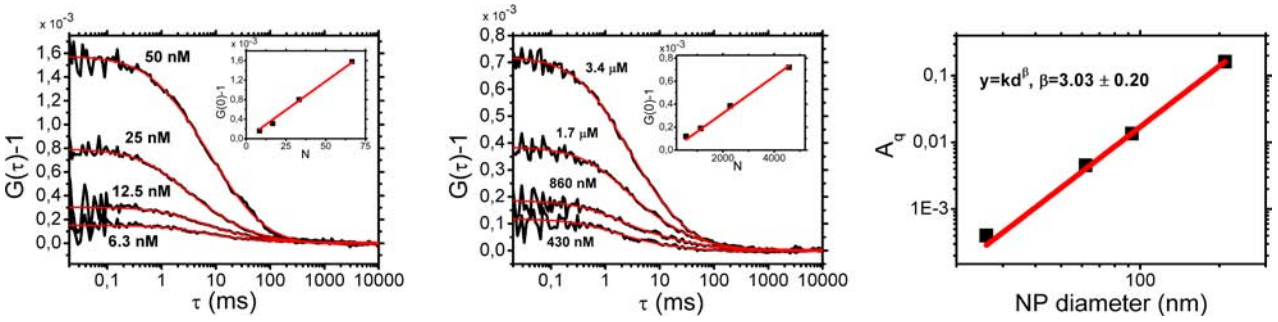

Figure 2. ACF curves from four measurements on (left) 62 nm and (middle) 26 nm diameter unlabeled NPs. Insets: Plots of $G(0) - 1$ vs N for the respective NP sizes. The value of A_q for each NP size was obtained from the slope of this plot, which is equal to A_q^2. (right) Plot of A_q vs NP diameter for the four NP sizes. A_q scaled with the NP volume (as indicated by the value of β), evidencing that the fluctuations were caused by interference.

of the detected power P is $\delta P = P_{tot} A_q \sqrt{N}$, since the standard deviation of N is $\delta N = \sqrt{N}$ because N is Poisson-distributed. The mean detected power $\langle P \rangle$ is dominated by the transmitted light and can be approximated as P_{tot}. Insertion into eq 1 gives

$$G(0) - 1 = \frac{P_{tot}^2 A_q^2 N}{P_{tot}^2} = A_q^2 N \qquad (2)$$

First, measurements were performed on polystyrene NPs diluted to concentrations such that on average $N = 0.18$ NPs resided in the detection volume. For 93 nm NPs, negative fluctuations in the detected laser light were directly visible in the intensity trace (Figure 1B), while a measurement on pure buffer solution showed only laser noise (Figure 1D,E). The histogram of the detected intensity for 93 nm NPs showed a broader distribution with a tail toward fewer counts per bin (Figure 1C), indicating that NPs transiting the detection volume gave rise to negative fluctuations.[11] Positive fluctuations may also have been present, but this could not be concluded given the limited signal-to-noise (S/N) ratio in these measurements.

Next, the dependence of the ACF amplitude on the particle concentration was investigated by measurements on unlabeled NPs with diameters of 210, 93, 62 (Figure 2 left), and 26 nm (Figure 2 middle). In agreement with eq 2, the ACF amplitudes scaled linearly with particle concentration. The resulting slopes of plots of $G(0) - 1$ versus N (insets in Figure 2) gave A_q values of 0.162 (210 nm NPs; data not shown), 0.0135 (93 nm; data not shown), 4.5×10^{-3} (62 nm), and 4.0×10^{-4} (26 nm). When a plot of these different A_q values against the NP diameter d is fitted to the function $A_q = kd^{\beta}$, an exponent β close to 3 should be obtained. Such a fit yielded $\beta = 3.03 \pm 0.20$ (Figure 2 right), and accordingly, the fluctuations scaled with the NP volume. This indicates that the observed fluctuations were caused by interference of the scattered light with the transmitted light, in contrast to scattering alone, which scales as the square of the polarizability and hence as the square of the volume.[3,5,7]

The particle-size dependence of the ACF curve decay time was investigated by measurements on the 210, 93, 62, and 26 nm diameter NPs. The respective diffusion times (τ_D) were 26, 8.6, 6.4, and 2.8 ms (Figure 3 top). From these diffusion times of NPs with known diameters, the radius of the detection volume was calculated to be $\omega_0 = 0.43\ \mu m \pm 0.015\ \mu m$ using the Stokes–Einstein equation; this gave a detection volume (V_{dv}) of 2.21 fL (the 210 nm NPs were too large to be considered pointlike[12] and were not used for estimation of ω_0).

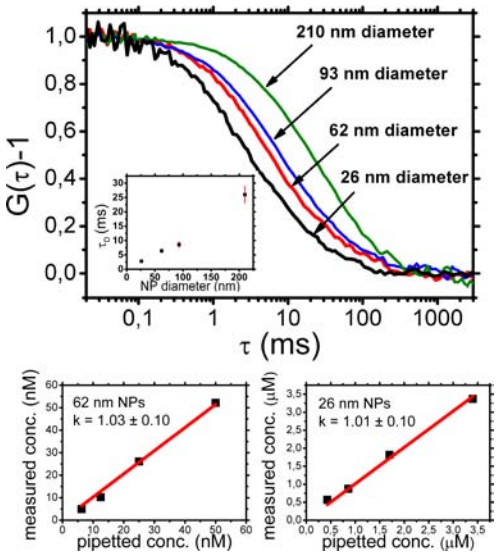

Figure 3. (top) Normalized ACF curves from measurements on NPs of different sizes, with diffusion times $\tau_D = 2.8$, 6.4, 8.6, and 26 ms, respectively. Inset: plot of τ_D vs NP diameter for the four NP sizes. Measurement times were 60 s. (bottom) Plots of measured vs pipetted concentrations of (left) 62 and (right) 26 nm NPs.

For spherical particles, the diffusion coefficient gives a separate estimate of the particle size (independent on A_q) that can be used together with eq 2 to derive the particle concentration from the ACF amplitude. In cases with homogeneous samples of known refractive index, the instrument can even be calibrated to yield the diffusion time, normalized effective cross section A_q, and concentration of an unknown sample by utilizing the facts that the diffusion time for pointlike particles depends linearly on the particle diameter d and that A_q scales as d^3. By calibrating the instrument using $A_q = 4.0 \times 10^{-4}$ and $\tau_D = 2.8$ ms for the 26 nm NPs, the diffusion time and A_q value for the 62 nm NPs could be predicted; these predictions were then used to convert the ACF amplitudes of the 62 nm NPs into concentrations. The result are shown for the 62 nm NPs (Figure 3 bottom left) and also for the 26 nm NPs used as the calibration standard (Figure 3 bottom right).

SICS measurements were also performed on unlabeled M13 bacteriophages. M13 is a filamentous-type bacteriophage having a length of 880 nm, a diameter of 6.6 nm, and a persistence length of ~2.2 μm;[13] M13 thus has the form of a rod. Measurements were performed at concentrations of ~10^{12}

dx.doi.org/10.1021/ja308213q | J. Am. Chem. Soc. 2012, 134, 19516–19519

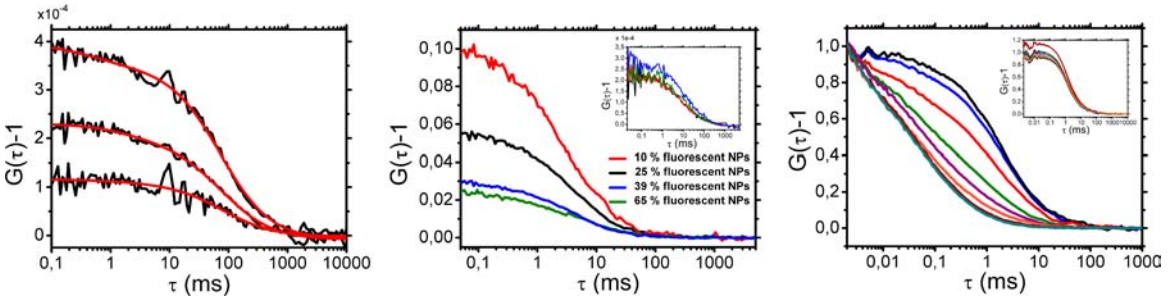

Figure 4. (left) SICS measurements on unlabeled M13 bacteriophages at specified concentrations of 10^{12} (upper curve), 5×10^{11} (middle curve), and 2.5×10^{11} phages/mL (lower curve). Oscillations are due to laser noise. (middle) SICS–FCS analysis of four mixtures of labeled (24 nm) and unlabeled (26 nm) NPs. The FCS curves indicate a varying labeled fraction, while the SICS curves (inset) display a fairly constant total NP concentration of ~500 nM. (right) FCS curves for binding of unlabeled 62 nm polystyrene NPs to ligands in the form of the positively charged HL488 fluorophore at varying concentrations. Inset: The corresponding SICS curves give the total NP concentration, allowing K_d to be estimated from each single measurement. Measurement times were 60 s.

viable phages/mL (~1.7 nM), which should correspond to a mean number of phages in the detection volume of $N = 2.2$. On the basis of an estimated polarizability[14] of the phages given by $4\pi\varepsilon_0(5.1 \times 10^{-18}\ \mathrm{cm}^3)$, the amplitudes in Figure 4 together with eq 2 indicate a concentration of $\sim 3 \times 10^{12}$ phages/mL (Figure 4 left; see the Supporting Information for detailed calculations). This is within the specified range of $\sim 10^{12}$ phages/mL because the total number of phages may be higher than the estimated number of viable phages.

Finally, SICS was combined with FCS. Mixtures of 26 nm nonfluorescent and 24 nm fluorescent NPs containing 10, 25, 39, and 65% fluorescent NPs with a constant total NP concentration were prepared. Analysis of the SICS curves indicated that the total NP concentration was constant at ~500 nM (inset of Figure 4 middle), while FCS analysis of the fluorescent fraction as expected indicated a larger variation (Figure 4 middle). The combined SICS–FCS analysis indicated that 9, 22, 35, and 64% of the NPs in the respective samples were fluorescent, in good agreement with the pipetted fractions. SICS–FCS was also used to measure the affinity of 62 nm negatively charged nonfluorescent NPs to ligands in the form of the positively charged fluorophore HL488 at pH 7.3 (Figure 4 right). Nonfluorescent NPs at a concentration of 55 nM were mixed with ligands at concentrations varying from 8 μM down to 1 nM, and each sample was analyzed by SICS–FCS. The FCS curves give the concentrations of free ligand, [L], and ligand–NP complexes, [L*NP], while the SICS curves give the total concentration of NPs. Thus, the dissociation constant K_d = [NP][L]/[L*NP] can be measured from each single measurement, which is not possible using single-color FCS. The eight measurements yielded $K_d = 3.1 \pm 3.6$ μM (Figure 4 right).

The fluctuations detected in SICS scale with the NP volume (Figure 2 right), which indicates that they are caused by interference of the forward-scattered laser light with the transmitted laser light.[3,5,7] Similar interference signals have been utilized for detection of single NPs,[15] for NP correlation analysis,[16] and in phase-analysis light scattering for measurement of particle velocity.[17] Also in PCS[9] and PhACS,[10] the generated signal is attributed to interference between the scattered and transmitted light, although a recent alternative theory interprets the photothermal fluctuations as originating from a nanolensing effect.[18]

The S/N ratio should increase as the square root of the laser power, and accordingly, use of photodiodes that can sustain count rates higher than 10^{16} Hz should substantially enhance the S/N ratio and sensitivity in SICS.

In principle, it should be possible to obtain the normalized effective cross section A_q by performing multicomponent analysis of intensity distribution histograms (Figure 1C).[11] Such analysis will be important for very nonspherical particles, whose sizes cannot be estimated from the diffusion coefficient. For such particles, comparison of A_q with the diffusion coefficient will then yield information about the particles' shape.[19] For the elongated M13 phages, the theoretically estimated A_q (see above) corresponds to that of a sphere with a diameter of 70 nm. Such a sphere would have had a diffusion time of 7–8 ms in the instrument used here, but the measured diffusion times of the phages were almost 10 times longer, indicating an extremely elongated shape.[19]

A related technique is inverse FCS,[12,20,21] which also combines analysis of labeled and unlabeled NPs. Inverse FCS allows the absolute volume of particles and even protein molecules in solution to be measured using zero-mode waveguides.[11] However, SICS as presented here has the advantage that NPs and possibly biomolecules can be analyzed in a simpler diffraction-limited detection volume.

In summary, when the refractive index is known, SICS allows analysis of both the size and concentration of unlabeled nanoparticles in solution. Furthermore, simultaneous analysis of labeled and unlabeled nanoparticles was shown by combining SICS and FCS. Measurements were performed on M13 phage viruses and on unlabeled and labeled polystyrene NPs with diameters as low as 24 nm. The contrast in SICS likely arises from interference between the scattered light from particles and the transmitted laser light, as indicated by the fact that the fluctuations scale with the particle volume.

The combination of SICS and FCS allows the percentage of label-carrying particles or viruses to be determined and enables single-measurement estimation of K_D even though only one species is labeled. The discussed possibilities for improvement should allow analysis of even smaller NPs and possibly biomolecules, which for example would allow the success of post-translational labeling of protein molecules to be measured.

■ ASSOCIATED CONTENT

Supporting Information

Materials and Methods and Discussion. This material is available free of charge via the Internet at http://pubs.acs.org.

dx.doi.org/10.1021/ja308213q | J. Am. Chem. Soc. 2012, 134, 19516–19519

AUTHOR INFORMATION

Corresponding Author
stewen@kth.se

Notes
The authors declare no competing financial interest.

ACKNOWLEDGMENTS

We are very grateful to Sebastian Grimm and Per-Åke Nygren for providing the M13 phages and to Daniel Johansson (Karolinska Institutet) and Per Thyberg for helpful discussions.

REFERENCES

(1) Berne, B. J.; Pecora, R. *Dynamic Light Scattering*; Wiley: New York, 1976.
(2) Swithenbank, J.; Beer, J. M.; Taylor, D. S.; Abbott, D.; McCreath, G. C. *Prog. Astronaut. Aeronaut.* **1977**, *53*, 421.
(3) Ignatovich, F. V.; Novotny, L. *Phys. Rev. Lett.* **2006**, *96*, No. 013901.
(4) Mitra, A.; Deutsch, B.; Ignatovich, F.; Dykes, C.; Novotny, L. *ACS Nano* **2010**, *4*, 1305.
(5) Zijlstra, P.; Orrit, M. *Rep. Prog. Phys.* **2011**, *74*, No. 106401.
(6) Person, S.; Deutsch, B.; Mitra, A.; Novotny, L. *Nano Lett.* **2011**, *11*, 257.
(7) Lindfors, K.; Kalkbrenner, T.; Stoller, P.; Sandoghdar, V. *Phys. Rev. Lett.* **2004**, *93*, No. 037401.
(8) Berciaud, S.; Cognet, L.; Blab, G. A.; Lounis, B. *Phys. Rev. Lett.* **2004**, *93*, No. 257402.
(9) Paulo, P. M. R.; Gaiduk, A.; Kulzer, F.; Krens, S. F. G.; Spaink, H. P.; Schmidt, T.; Orrit, M. *J. Phys. Chem. C* **2009**, *113*, 11451.
(10) Octeau, V.; Cognet, L.; Duchesne, L.; Lasne, D.; Schaeffer, N.; Fernig, D. G.; Lounis, B. *ACS Nano* **2009**, *3*, 345.
(11) Sandén, T.; Wyss, R.; Santschi, C.; Hassaïne, G.; Deluz, C.; Martin, O. J. F.; Wennmalm, S.; Vogel, H. *Nano Lett.* **2012**, *12*, 370.
(12) Wennmalm, S.; Thyberg, P.; Xu, L.; Widengren, J. *Anal. Chem.* **2009**, *81*, 9209.
(13) Purdy, K. R.; Fraden, S. *Phys. Rev. E* **2004**, *70*, No. 061703.
(14) Zhu, H. Y.; White, I. M.; Suter, J. D.; Zourob, M.; Fan, X. D. *Analyst* **2008**, *133*, 356.
(15) Batchelder, J. S.; Taubenblatt, M. A. *Appl. Phys. Lett.* **1989**, *55*, 215.
(16) Hilbert, M.; Hippchen, H.; Wehling, A.; Walla, P. J. *J. Phys. Chem. B* **2005**, *109*, 18162.
(17) Miller, J. F.; Schatzel, K.; Vincent, B. *J. Colloid Interface Sci.* **1991**, *143*, 532.
(18) Selmke, M.; Braun, M.; Cichos, F. *ACS Nano* **2012**, *6*, 2741.
(19) Tirado, M. M.; Martinez, C. L.; Delatorre, J. G. *J. Chem. Phys.* **1984**, *81*, 2047.
(20) Wennmalm, S.; Widengren, J. *Anal. Chem.* **2010**, *82*, 5646.
(21) Wennmalm, S.; Widengren, J. *Front. Biosci.* **2011**, *S3*, 385.